Dynamical analysis of a chemostat model for 4-chlorophenol and sodium salicylate mixture biodegradation

Neli Dimitrova

Institute of Mathematics and Informatics,
Bulgarian Academy of Sciences, Bulgaria
nelid@math.bas.bg   0000-0002-4722-6440

Abstract: **We consider a mathematical continuous-time model for biodegradation of 4-chlorophenol and sodium salicylate mixture by the microbial strain *Pseudomonas putida* in a chemostat. The model is described by a system of three nonlinear ordinary differential equations and is proposed for the first time in the paper [Y.-H. Lin, B.-H. Ho, Biodegradation kinetics of phenol and 4-chlorophenol in the presence of sodium salicylate in batch and chemostat systems, *Processes*, 10:694, 2022], where the model is only quantitatively verified. This paper provides a detailed analysis of the system dynamics. Some important basic properties of the model solutions like existence, uniqueness and uniform boundedness of positive solutions are established. Computation of equilibrium points and study of their local asymptotic stability and bifurcations in dependence of the dilution rate as a key model parameter are also presented. Thereby, particular intervals for the dilution rate are found, where one or three interior (with positive components) equilibrium points do exist and possess different types of local asymptotic stability/instability. Hopf bifurcations are detected leading to the occurrence of stable limit cycles around some interior equilibrium points. A transcritical bifurcation also exists and implies stability exchange between an interior and the boundary (washout) equilibrium. The results are illustrated by lots of numerical examples.**

Keywords: **4-chlorophenol and sodium salicylate mixture, Biodegradation, Chemostat model, SKIP kinetics, Equilibrium points, Stability analysis, Hopf bifurcations, Numerical simulation**

I. INTRODUCTION

Phenol, phenolic derivatives and their mixtures are among the extremely toxic pollutants, arising as effluents from many industrial processes and affecting the environment and the human health [1, 2]. Sodium salicilate (SA) is recently also qualified as a typical contaminant in wastewater although its usage as a drug derivative in medicine and as preservative in foods production (cf. e. g. [3] and the references therein). Among the many effluent treatment processes like chemical, physical, physicochemical, etc., biological degradation of chemical organic mixtures is known to be the most effective and efficient technology in terms of costs, time and performance. Various specific microorganisms such as *Aspergillus awamori*, *Arthrobacter*, *Candida tropicalis*, *Gliomastix indicus*, *Pseudomonas putida*, *Rhodococcus*, *Trametes hirsute*, and many others are recently successfully used to degrade the pollutants up to prescribed ecological norms [4–10]. Microorganisms ability to remove toxic organic compounds has been mostly studied at lab-scales in batch systems, whereas investigations performed in continuous-time systems (continuously stirred bioreactors or chemostats) are of much smaller number.

One of the most important characteristics in chemostat cultivation is the dilution rate D. In practice, D

is defined as the flow of medium per time over the volume of the culture in the reactor and can be directly manipulated by the experimenter. For that reason a large number of studies is devoted to investigate the effect of D on the long-term behavior of the chemostat dynamics. Among the rich literature we can mention e. g. the books [11,12]. Using D as a control parameter is considered in [13–15] and applied to a bioreactor model for simultaneous degradation of phenol and *p*-cresol [13,14] as well as of phenol and SA mixture [15] in industrial wastewater.

Biodegradation of 4-chlorophenol (4-CP) and SA mixture by the strain *Pseudomonas putida (P. putida)* is reported in [16–19], where series of batch tests are conducted and used to determine the parameters in the kinetic growth models. The high biodegradation rate of 4-CP and SA by *P. putida* is established in details by Lin and Ho in [10]. Experimental results show that *P. putida* cells are not able to degrade 4-CP alone due to its toxicity. However, the addition of SA to 4-CP significantly enables the biodegradation of the whole mixture by *P. putida* microorganisms. The authors present in their paper [10] for the first time a continuous-time (chemostat) model for biodegradation of the 4-CP and SA mixture by the strain *P. putida*. It is shown that the experimental results in the chemostat system fit well with the model prediction for a particular value of the dilution rate $D = 0.04$.

Here we consider the chemostat model for biodegradation of 4-CP and SA mixture by the strain *P. putida* proposed in [10]. To our knowledge, till now this model has not yet been investigated mathematically. This paper aims to perform a detailed qualitative analysis of the model solutions.

The paper is structured in the following way. Section II presents shortly the mathematical model for biodegradation of 4-chlorophenol and sodium salicylate mixture by the strain *Pseudomonas putida*, taken from [10].

Section III reports on basic and important properties of the model solutions, namely existence and uniform boundedness of nonnegative solutions.

Section IV is devoted to computation of the equilibrium points and investigation of their local asymptotic stability. Depending on the values of the parameter D it is shown numerically, that the model can possess up to three interior (with positive components) and one boundary (washout with respect to biomass) equilibrium points.

Section V presents numerical examples as illustration of the model dynamics. All calculations in Sections IV and V are carried out in the computer algebra system

Maple using its computational and visualization tools.

The last Section VI contains discussion and some concluding remarks.

II. THE CHEMOSTAT MODEL

The chemostat model for biodegradation of the binary mixture of 4-chlorophenol (4-CP) and sodium salicylate (SA) by the strain *Pseudomonas putida*, proposed and experimentally validated in [10], is described by the following system of nonlinear ordinary differential equations

$$\frac{dS_A(t)}{dt} = D(S_A^0 - S_A(t))$$
$$- \mu_{SA}(S_A(t), S_{CP}(t))X(t), \quad (1)$$
$$\frac{dS_{CP}(t)}{dt} = D(S_{CP}^0 - S_{CP}(t))$$
$$- \mu_{CP}(S_{CP}(t))X(t), \quad (2)$$
$$\frac{dX(t)}{dt} = (\mu_X(S_A(t), S_{CP}(t)) - D) X(t), \quad (3)$$

where $\mu_{SA}(S_A, S_{CP})$ and $\mu_{CP}(S_{CP})$ are the degradation rates of sodium salicylate (SA) and 4-chlorophenol (4-CP) by the strain *P. putida*, and $\mu_X(S_A, S_{CP})$ is the specific growth rate of *P. putida* cells on binary substrates SA and 4-CP. These kinetic functions are described by the following analytical expressions [10]

$$\mu_{SA} = \mu_{SA}(S_A, S_{CP}) = \frac{k_A S_A}{K_{SA} + S_A + \frac{S_A^2}{K_{I,A}} + \frac{S_{CP}^2}{I_{CP}}},$$

$$\mu_{CP} = \mu_{CP}(S_{CP}) = \frac{k_C S_{CP}}{K_{CP} + S_{CP} + \frac{S_{CP}^2}{K_{I,CP}}},$$

$$\mu_X = \mu_X(S_A, S_{CP}) = \frac{\mu_{m,A} S_A}{K_{SA} + S_A + \frac{S_A^2}{K_{I,A}}}$$
$$- k_{d,A}(1 + m_{d,CP} S_{CP}).$$

The meaning of the state variables S_A, S_{CP}, X and of the model parameters is summarized in Table I. The numerical values in the last column are obtained by laboratory experiments and given in [10].

The function $\mu_{SA}(S_A, S_{CP})$ presents the so called SKIP (Sum Kinetics with Interaction Parameters, cf. [4]) model, where the SA utilization is inhibited by 4-CP, $\mu_{CP}(S_{CP})$ is described by the well known Haldane law, and does not incorporate inhibition by SA. The specific growth rate $\mu_X(S_A, S_{CP})$ is presented as a difference of a Haldane function and a second term, representing the toxicity of 4-CP on the *P. putida* cells by a maintenance/death quantity: $k_{d,A}$ is the endogenous decay coefficient of cells on SA alone, and $m_{d,CP}$ is a decay constant due to 4-CP (cf. [10] and the

Table I: Model variables and parameters

	Definition	Value
S_A	Sodium salicylate (SA) concentration [mg/L]	–
S_{CP}	4-chlorophenol (4-CP) concentration [mg/L]	–
X	Cells concentration [mg/L]	–
D	Dilution rate [h^{-1}]	–
S_A^0	Influent SA concentration [mg/L]	85
S_{CP}^0	Influent 4-CP concentration [mg/L]	12
k_A	Maximum specific degradation rate of SA by cells [mg SA/mg cell-h]	0.564
K_{SA}	Half-saturation constant of SA [mg/L]	71.7
$K_{I,A}$	Inhibition constant of SA [mg/L]	3178.2
I_{CP}	Interaction parameter of 4-CP to SA [mg/L]	0.355
k_C	Maximum specific degradation rate of 4-CP by cells [mg 4-CP/mg cell-h]	0.189
K_{CP}	Half-saturation constant of 4-CP [mg/L]	1.106
$K_{I,CP}$	Inhibition constant of 4-CP [mg/L]	0.977
$\mu_{m,A}$	Maximum specific growth rate of cells on SA [h^{-1}]	0.247
$k_{d,A}$	Decay coefficient of cells on SA [h^{-1}]	1.635×10^{-4}
$m_{d,CP}$	Decay constant due to 4-CP [L/mg]	6.11

references therein). It is shown in [10] that these kinetic models give a good fit to the experimental results of 4-CP and SA biodegradation for a particular value of $D = 0.04$.

III. BASIC PROPERTIES OF THE MODEL SOLUTIONS

In this section we investigate important properties of the solutions of system (1)–(3) ensuring adequacy of the dynamic model and its ability to describe a real-life process.

Theorem 1. *The nonnegative cone and the interior of the nonnegative cone in $\mathbb{R}^3$ are positively invariant for the model (1)–(3).*

Proof: If $X(\tau) = 0$ at some time moment $\tau \geq 0$ then equation (3) implies that $X(t) = 0$ for all $t \geq 0$ due to uniqueness of solutions of Cauchy's problem (cf. e. g. [20], Chapter 1). Then the model reduces to

$$\frac{dS_A(t)}{dt} = D(S_A^0 - S_A(t)),$$
$$\frac{dS_{CP}(t)}{dt} = D(S_{CP}^0 - S_{CP}(t)),$$

which solutions are

$$S_A(t) = S_A^0 + (S_A^0 - S_A(0))e^{-Dt},$$
$$S_{CP}(t) = S_{CP}^0 + (S_{CP}^0 - S_{CP}(0))e^{-Dt}.$$

Obviously, $S_A(t) \to S_A^0$ and $S_{CP}(t) \to S_{CP}^0$ exponentially as $t \to \infty$. Thus the face $\{S_A \geq 0, S_{CP} \geq 0, X = 0\}$ is invariant under the flow (1)–(3).

If $X(0) > 0$ then by equation (3) it follows

$$X(t) = X(0)e^{\int_0^t (\mu_X(S_A(\theta), S_{CP}(\theta)) - D)d\theta},$$

which means that $X(t) > 0$ for all $t > 0$.

If $S_A(\tau) = 0$ for some $\tau \geq 0$ then equation (1) implies $\dfrac{dS_A(t)}{dt} = DS_A^0 > 0$.

Similarly, if $S_{CP}(\tau) = 0$ for some $\tau \geq 0$ then by equation (2), $\dfrac{dS_{CP}(t)}{dt} = DS_{CP}^0 > 0$ holds true. Therefore the vector field of (1)–(3) points inside the positive cone in $\mathbb{R}^3$, i. e. all model solutions are positive. This completes the proof of Theorem 1. ∎

Denote

$$\Omega = \{(S_A, S_{CP}, X) : S_A > 0, S_{CP} > 0, X > 0\}.$$

In what follows we shall consider initial conditions for (1)–(3) in Ω.

In the proof of the next theorem we need the following assumption.

Assumption A1. There exist a time moment $T > 0$ so that the inequality

$$\mu_X(S_A(t), S_{CP}(t)) \leq \mu_{SA}(S_A(t), S_{CP}(t))$$

is fulfilled for all time $t \geq T$.

Remark. Assumption A1 is technical and is used in the proof of Theorem 2. It can also be justified by the following reasoning. As already mentioned before, the *P. putida* cells could not degrade the 4-CP alone due to the strong toxicity of the latter, which is described by the term $-k_{d,A}(1 + m_{d,CP}S_{CP})$ in the expression
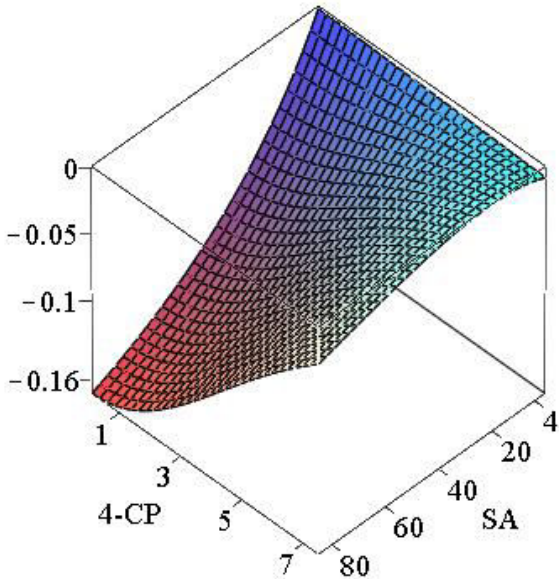
Fig. 1: Graph of the function $\mu_X(S_A, S_{CP}) - \mu_{SA}(S_A, S_{CP})$ for $S_A \in [0.1, S_A^0]$, $S_{CP} \in [0.1, 7.5]$.

of $\mu_X(S_A, S_{CP})$ (cf. [10] and the references therein). For that reason SA is used as growth substrate for the cometabolic biodegradation of 4-CP by *P. putida* cells [16]. Moreover, the growth rate of SA should be higher to neutralize the toxicity of 4-CP and in this way to enable the growth of the microorganisms and their ability to degrade both SA and 4-CP in the culture medium. For the specific growth rate of cells on SA alone in the absence of 4-CP (i. e. with $S_{CP} = 0$), using the fact that $\mu_{m,A} < k_A$ (see Table I) we obtain

$$\mu_X(S_A, 0) - \mu_{SA}(S_A, 0) = \frac{(\mu_{m,A} - k_A)S_A}{K_{SA} + S_A + \frac{S_A^2}{K_{I,A}}} - k_{d,A} < 0.$$

It is then reasonable to expect that appropriate reduced values of $S_{CP} < S_{CP}^0$ do exist which could retain the inequality $\mu_X(S_A, S_{CP}) \leq \mu_{SA}(S_A, S_{CP})$ after some time moment T, so that Assumption A1 is meaningful. Using the numerical coefficient values in Table I, Figure 1 shows an example where the difference $\mu_X(S_A, S_{CP}) - \mu_{SA}(S_A, S_{CP})$ is negative if $S_{CP} \leq 7.5 < S_{CP}^0 = 12$.

Theorem 2. *Let Assumption A1 be fulfilled. Then for any starting point $(S_A(0), S_{CP}(0), X(0)) \in \Omega$, all model solutions are uniformly bounded and thus exist for all time $t > 0$.*

Proof: From equation (2) we have

$$\frac{dS_{CP}(t)}{dt} = D(S_{CP}^0 - S_{CP}(t)) - \mu_{CP}(S_{CP}(t))X(t)$$
$$\leq D(S_{CP}^0 - S_{CP}(t)).$$

Multiplying both sides of the latter inequality by e^{Dt} we obtain consecutively

$$e^{Dt}\frac{dS_{CP}(t)}{dt} + e^{Dt}DS_{CP}(t) \leq e^{Dt}DS_{CP}^0,$$
$$\frac{d}{dt}\left(e^{Dt}S_{CP}(t)\right) \leq e^{Dt}DS_{CP}^0,$$
$$\int_0^t \frac{d}{d\xi}\left(e^{D\xi}S_{CP}(\xi)\right)d\xi \leq DS_{CP}^0\int_0^t e^{D\xi}d\xi,$$
$$e^{Dt}S_{CP}(t) - S_{CP}(0) \leq S_{CP}^0(e^{Dt} - 1),$$
$$S_{CP}(t) \leq e^{-Dt}S_{CP}(0) + S_{CP}^0(1 - e^{-Dt}).$$

The last inequality implies $\lim \sup_{t\to\infty} S_{CP}(t) \leq S_{CP}^0$. Since $S_{CP}(t)$ is positive, it follows that it is uniformly bounded and thus exists for all time $t \in (0, +\infty)$.

Since $S_A(t)$, $S_{CP}(t)$ are positive for all $t > 0$, it follows that $\mu_{SA}(S_A(t), S_{CP}(t))$ is also positive for all $t > 0$. Using equation (1), in a similar way as above we obtain

$$S_A(t) \leq e^{-Dt}S_A(0) + S_A^0(1 - e^{-Dt}),$$

which means that $\lim \sup_{t\to\infty} S_A(t) \leq S_A^0$, i. e. $S_A(t)$ is uniformly bounded and exists for all time $t \in (0, +\infty)$.

Suppose now that Assumption A1 is fulfilled, i. e. there exists a time moment $T > 0$, so that

$$\mu_X(S_A(t), S_{CP}(t)) - \mu_{SA}(S_A(t), S_{CP}(t)) \leq 0$$

for each $t \geq T$ is valid. Denote $W(t) = S_A(t) + X(t)$. Then by equations (1) and (3) we obtain

$$\frac{dW(t)}{dt} = \frac{d}{dt}S_A(t) + \frac{d}{dt}X(t)$$
$$= D(S_A^0 - S_A(t)) - \mu_{SA}(S_A(t), S_{CP}(t))X(t)$$
$$\quad + \mu_X(S_A(t), S_{CP}(t))X(t) - DX(t)$$
$$= D(S_A^0 - S_A(t) - X(t)) + \mu_X(S_A(t), S_{CP}(t))X(t)$$
$$\quad - \mu_{SA}(S_A(t), S_{CP}(t))X(t)$$
$$\leq D(S_A^0 - W(T)).$$

The latter inequality implies that

$$W(t) \leq S_A^0 + (W(0) - S_A^0)e^{-Dt} \text{ for all } t \geq T,$$

which means that $\lim \sup_{t\to\infty} W(t) \leq S_A^0$. Since S_A and X are positive, and S_A is upper bounded, the latter inequality shows that $X(t)$ is uniformly bounded as well and thus exists for all time $t \geq 0$. This completes the proof of Theorem 2. $\blacksquare$

IV. Equilibrium Points and their Local Asymptotic Stability

The equilibrium points of model (1)–(3) are solutions with respect to (S_A, S_{CP}, X) of the following nonlinear algebraic system, obtained from (1)–(3) by setting in the latter the right-hand sides equal to zero:

$$D(S_A^0 - S_A) - \mu_{SA}(S_A, S_{CP})X = 0, \qquad (4)$$

$$D(S_{CP}^0 - S_{CP}) - \mu_{CP}(S_{CP})X = 0, \qquad (5)$$

$$(\mu_X(S_A, S_{CP}) - D)X = 0. \qquad (6)$$

Substituting $S_A = S_A^0$, $S_{CP} = S_{CP}^0$ in equations (4)–(5) obviously leads to $X = 0$ for any $D > 0$. We denote this equilibrium point by $E_0 = (S_P^0, S_A^0, 0)$ and call it boundary or washout equilibrium.

Assume that $X \neq 0$. The third equation (6) implies

$$\mu_X(S_A, S_{CP}) - D = 0.$$

Substituting in the latter $S_A = S_A^0$ and $S_{CP} = S_{CP}^0$ we obtain

$$\mu_X(S_A^0, S_{CP}^0) = D.$$

This value of D also leads to $X = 0$ as an equilibrium component of the model. We denote

$$D_{\max} := \mu_X(S_A^0, S_{CP}^0).$$

Using the numerical values in Table I we get

$$D_{\max} \approx 0.11991488.$$

In what follows we shall show by numerical computations that there exist one or three interior equilibria in dependance of D in different subintervals of $(0, D_{\max})$. The computations are carried out in the computer algebra system *Maple* using the procedure `solve` for solving a system of nonlinear algebraic equations. We proceed in the following way. A mesh of points $\{D_j\}$ in the interval $(0, D_{\max}]$ is constructed and for each value $D = D_j$ the system (4)–(6) is solved numerically, looking for solutions (S_A, S_{CP}, X), such that $0 < S_A \leq S_A^0$, $0 < S_{CP} \leq S_{CP}^0$, $X > 0$. These solutions will be called admissible. The numerical computations deliver that there exist four values of D, $0 < D_1 < D_2 < D_3 < D_4 < D_{\max}$,

$$D_1 \approx 0.09348963, \qquad D_2 \approx 0.095396073,$$
$$D_3 \approx 0.09539752, \qquad D_4 \approx 0.0960529898,$$

such that

(i) If $D \in (0, D_1)$ then there exists a unique interior admissible equilibrium.

(ii) If $D \in [D_1, D_2] \cup (D_2, D_3]$ then there exist three admissible interior equilibrium points.

(iii) If $D \in (D_3, D_4] \cup (D_4, D_{\max})$ then there exists a unique admissible interior equilibrium.

(iv) If $D \geq D_{\max}$ then the washout equilibrium E_0 is the unique steady state.

More details on the existence of the equilibrium points will be given below after investigating their local asymptotic stability, see items (S1) to (S6).

The local asymptotic stability of an equilibrium point is determined by the signs of the real parts of the eigenvalues of the Jacobian evaluated at this equilibrium, or equivalently by the roots of the corresponding characteristic polynomial (cf. [21], Chapters 1 and 3).

The Jacobian $J = J(S_A, S_{CP}, X)$ related to equations (4)–(6) has the form

$$J =$$

$$\begin{pmatrix} -D - \frac{\partial \mu_{SA}}{\partial S_A}X & -\frac{\partial \mu_{SA}}{\partial S_{CP}}X & -\mu_{SA}(S_A, S_{CP}) \\ 0 & -D - \frac{\partial \mu_{CP}}{\partial S_{CP}}X & -\mu_{CP}(S_{CP}) \\ \frac{\partial \mu_X}{\partial S_A}X & -k_{d,A}m_{d,CP}X & \mu_X(S_A, S_{CP}) - D \end{pmatrix}$$

Denote by $|J - \lambda I_3| = \det(J - \lambda I_3)$ the characteristic polynomial of J evaluated at some equilibrium point, here I_3 is the 3-dimensional identity matrix, and λ is a complex number. Obviously, $|J - \lambda I_3|$ is a polynomial of 3rd degree with respect to λ, which always possesses one real root, the other two roots are either real or a pair of complex conjugate values. Consider first the characteristic polynomial $|J(E_0) - \lambda I_3|$ evaluated at the boundary equilibrium $E_0 = (S_A^0, S_{CP}^0, 0)$. It is straightforward to see that

$$|J(E_0) - \lambda I_3| = (-D - \lambda)^2 \left(\mu_X(S_A^0, S_{CP}^0) - D - \lambda\right)$$
$$= (D + \lambda)^2 (D_{\max} - D - \lambda).$$

Obviously, $\lambda_{1,2} = -D < 0$ are two real roots of the above characteristic polynomial. The third root is also real, $\lambda_3 = D_{\max} - D$, and its sign satisfies

$$\lambda_3 = D_{\max} - D \begin{cases} > 0, & \text{if } D < D_{\max}, \\ < 0, & \text{if } D > D_{\max}, \\ = 0, & \text{if } D = D_{\max}. \end{cases}$$

Therefore

$$E_0 \text{ is} \begin{cases} \text{locally asymptotically unstable} \\ \text{(\textit{unstable node}), if } D < D_{\max}, \\ \text{locally asymptotically stable} \\ \text{(\textit{stable node}), if } D > D_{\max}. \end{cases}$$

At $D = D_{\max}$ the eigenvalue λ_3 becomes equal to zero, so E_0 can undergo a bifurcation at this value of D.

The eigenvalues of each interior equilibrium point are determined numerically, using the already computed values of the corresponding equilibrium components on the mesh $\{D_j\}$. The computations are carried out in *Maple* using the facilities of the package `VectorCalculus` (the procedure `Jacobian`) and the package `LinearAlgebra` (procedure `CharacteristicPolynomial`) as well as `solve` for finding the solutions of the latter polynomial.

Let us remind, that one real root of the characteristic polynomial for each interior steady state is always negative, thus the corresponding local stability depends on the signs of the real parts of the other two roots. The numerical computations deliver the following results, which are described below in items (S1) to (S6).

(S1) If $D \in (0, D_1)$, then there is a unique admissible interior equilibrium E_1, and it is locally asymptotically stable. For relatively small values of D, E_1 has three negative real eigenvalues, so E_1 is *a stable node*. For values of D near to (but less than) D_1, two of the real eigenvalues are transformed into a pair of complex conjugate eigenvalues with negative real part, the third eigenvalue remains real and negative, thus E_1 is *a stable focus*.

At $D = D_1$, two new equilibrium points are 'born', $E_2 \equiv E_3 \approx (46.626, 3.121, 19.977)$, $E_1 \approx (44.789, 0.80632, 17.702)$.

(S2) If $D \in (D_1, D_2)$, then there exist three admissible equilibrium points, E_1, E_2 and E_3. The steady state E_1 is *a stable focus*, with one real negative eigenvalue and a pair of complex conjugate eigenvalues with negative real part. E_2 and E_3 are locally asymptotically unstable, E_2 is *a saddle*, having one positive and two negative real eigenvalues. For values of D near to (but greater than) D_1, E_3 is *a saddle* possessing one negative and two positive real eigenvalues, if D is close to (but less than) D_2, then E_3 becomes *a saddle-focus*, having one real negative eigenvalue and a pair of complex conjugate eigenvalues with positive real part.

At $D = D_2$, the pair of complex conjugate eigenvalues of E_1 crosses the imaginary axis form left to right, i. e. the real parts become equal to zero, so E_1 undergoes a *supercritical Hopf bifurcation*, leading to the occurrence of a stable limit cycle and sustainable oscillation around it thereafter.

(S3) If $D \in (D_2, D_3)$, then the three interior equilibrium points are locally asymptotically unstable. E_1

is *a saddle-focus* with one negative real eigenvalue and a pair of complex conjugate eigenvalues with positive real part. E_2 is *a saddle* having three real eigenvalues—one positive and two negative. E_3 is *a saddle-focus* with one negative real eigenvalue and a pair of complex conjugate eigenvalues with positive real part.

At $D = D_3$, the two equilibria E_1 and E_2 coalesce and disappear thereafter, so that only the equilibrium E_3 continues to exist for $D > D_3$.

(S4) If $D \in (D_3, D_4)$ then the unique admissible equilibrium E_3 is *a saddle-focus* (locally asymptotically unstable), having one real negative eigenvalue and a pair of complex conjugate eigenvalues with positive real part.

At $D = D_4$, the real parts of the complex conjugate eigenvalues of E_3 cross the imaginary axis from right to left (i. e. they become equal to zero), thus E_3 undergoes *a subcritical Hopf bifurcation*, leading to the occurrence of a stable limit cycle around E_3 just before D_4.

(S5) If $D \in (D_4, D_{\max})$ then the unique interior equilibrium E_3 is locally asymptotically stable. If D is near to (but greater than) D_4, then E_3 changes into *a stable focus* with one negative real eigenvalue and a pair of complex conjugate eigenvalues with negative real part.

For values of D relatively away from D_4 and near to $D_{\max}$, the pair of complex conjugate eigenvalues of E_3 is transformed into two negative real eigenvalues, so E_3 becomes *a stable node*.

At $D = D_{\max}$, the two equilibria E_3 and E_0 coincide and exchange stability, thus E_3 undergoes a *transcritical bifurcation*, leading to stability exchange between E_3 and E_0.

(S6) If $D > D_{\max}$ then the washout equilibrium E_0 is the unique locally asymptotically stable equilibrium of the model, having three real negative eigenvalues, i. e. E_0 is *a stable node*.

Items (S1) to (S6) are summarized in Table II for better visibility.

Figures 2, 3 and 4 visualize the equilibrium components of E_1, E_2 and E_3 and their local asymptotic stability. It is seen from these figures, that the inequalities $E_1 < E_2 < E_3$ are satisfied componentwise for all $D \in (D_1, D_3)$.

Below we will demonstrate the different stability types of the equilibrium points taking particular numerical values of the dilution rate D in accordance with items (S1) to (S6).

Table II: Stability and bifurcations of equilibrium points, where the following notations are used: StN—stable node, StF—stable focus, Sad-F—saddle-focus, Sad—saddle, SpHB—supercritical Hopf bifurcation, SbHB—subcritical Hopf bifurcation, TrB—transcritical bifurcation.

|	$(0, D_1)$	(D_1, D_2)	D_2	(D_2, D_3)	(D_3, D_4)	D_4	$(D_4, D_{\max})$	$D_{\max}$	$D > D_{\max}$
E_1	StN&StF	StF	SpHB	Sad-F	—	—	—	—	—
E_2	—	Sad	Sad	Sad	—	—	—	—	—
E_3	—	Sad&Sad-F	Sad-F	Sad-F	Sad-F	SbHB	StF&StN	TrB	—
E_0	Sad	Sad	Sad	Sad	Sad	Sad	Sad	TrB	StN
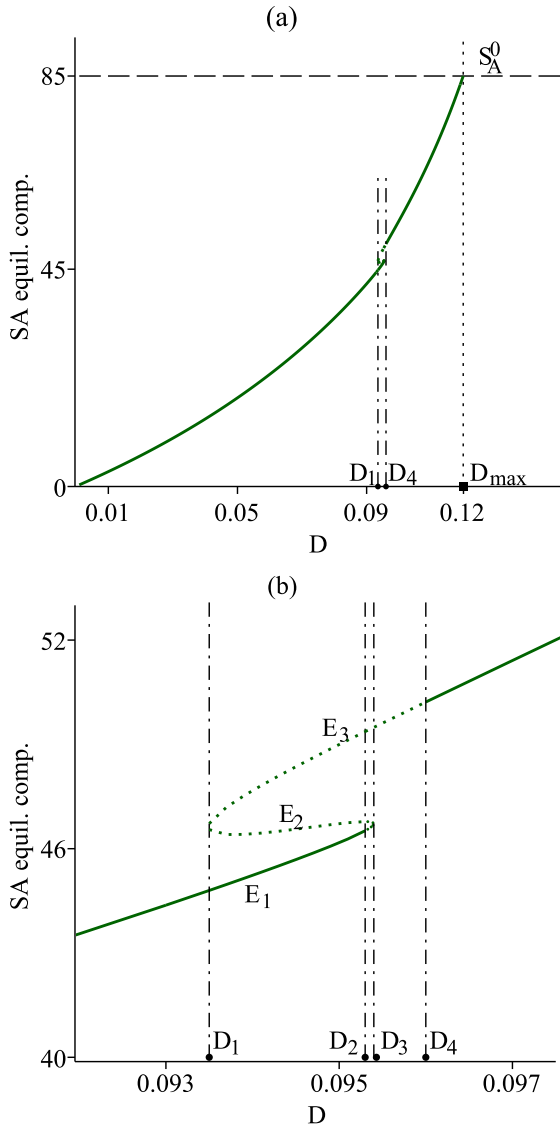
Fig. 2: (a) S_A-component of the interior equilibria for $D \in (0, D_{\max}]$. (b) Enlarged fragment of plot (a) in the region $[D_1, D_4]$. Solid lines mark the stable branches, and dotted lines mark the unstable branches of the equilibria.
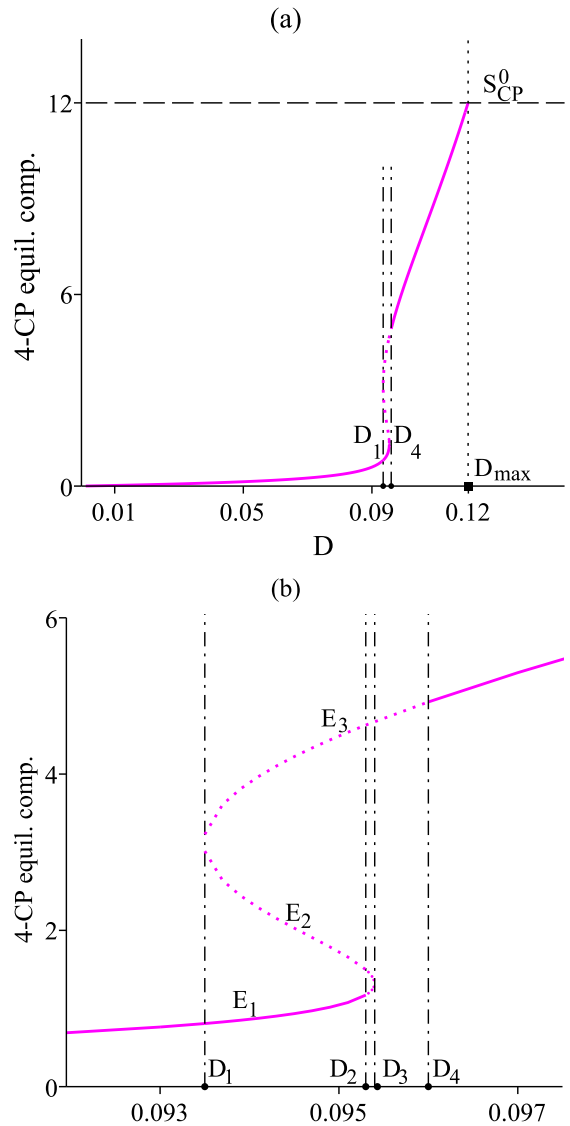
Fig. 3: (a) S_{CP}-component of the interior equilibria for $D \in (0, D_{\max}]$. (b) Enlarged fragment of plot (a) in the region $[D_1, D_4]$. Solid lines mark the stable branches, and dotted lines mark the unstable branches of the equilibria.

Fig. 4: (a) X-component of the interior equilibria for $D \in (0, D_{\max}]$. (b) Enlarged fragment of plot (a) in the region $[D_1, D_4]$. Solid lines mark the stable branches, and dotted lines mark the unstable branches of the equilibria.

V. NUMERICAL SIMULATION OF THE MODEL DYNAMICS

In this section we consider several numerical examples illustrating the dynamic behavior of the model solutions for different values of $D > 0$ according to items (S1) to (S6) and Table II. The simulations are fulfilled in *Maple* using the procedure DEplot in the package DEtools for solving a system of ODEs and visualizing its solutions and trajectories.

Example 1. $D = 0.04 \in (0, D_1) = (0, 0.09348963)$. According to item (S1), for this value of D there is a unique locally asymptotically stable equilibrium point

$$E_1 = (13.975632, 0.0990022, 30.911877), \textit{stable node},$$

having three real negative eigenvalues -0.040234675, -0.169519608, -4.377294035.

As already mentioned before, the model (1)–(3) has been validated only for this value of the dilution rate D in [10]. There, the authors state that the solutions approach in finite time the point $F = (7.3, 0.58, 39.2)$, called a steady state, but it is not so. Obviously, the components of F are quite different from the ones of E_1.

Figure 5 illustrates the time evolution of $S_A(t)$, $S_{CP}(t)$ and $X(t)$ with starting point $P_1(0) = (S_A(0), S_{CP}(0), X(0)) = (85, 12, 21)$, taken from [10]. It is seen that the solution curves cross (even twice by $X(t)$) or go close (to $S_A(t)$) to the dotted horizontal line corresponding to the point F, but do not stabilize around the latter. As expected, the solutions approach the stable node E_1 for sufficiently large time t.

Figures 6 and 7 demonstrate the attractivity of the equilibrium E_1 with more initial conditions in the set $\mathcal{P}_1(0) = \{(40, 0.2, 21), (9, 0.1, 25), (15, 0.01, 38), (20, 0.3, 42)\}$.

Example 2.
$D = 0.09345 \in (0, D_1) = (0, 0.09348963)$. For this value of D, relatively near to D_1 (see item (S1)), the equilibrium point is unique,

$$E_1 = (44.755915, 0.802484, 17.714725), \textit{ stable focus},$$

with one real negative eigenvalue and a pair of complex conjugate eigenvalues with negative real part: -0.326342, $-0.0695014 \pm 0.00448095i$.

Figures 8 and 9 illustrate the dynamic behavior of the model using the initial data in the set $\mathcal{P}_2(0) = \{(84, 11, 21), (11, 0.1, 25), (15, 4, 38), (20, 0.3, 42)\}$.

Example 3. $D = 0.09539 \in (D_1, D_2) = (0.09348963, 0.095396073)$. This value of D is near to (but less than)
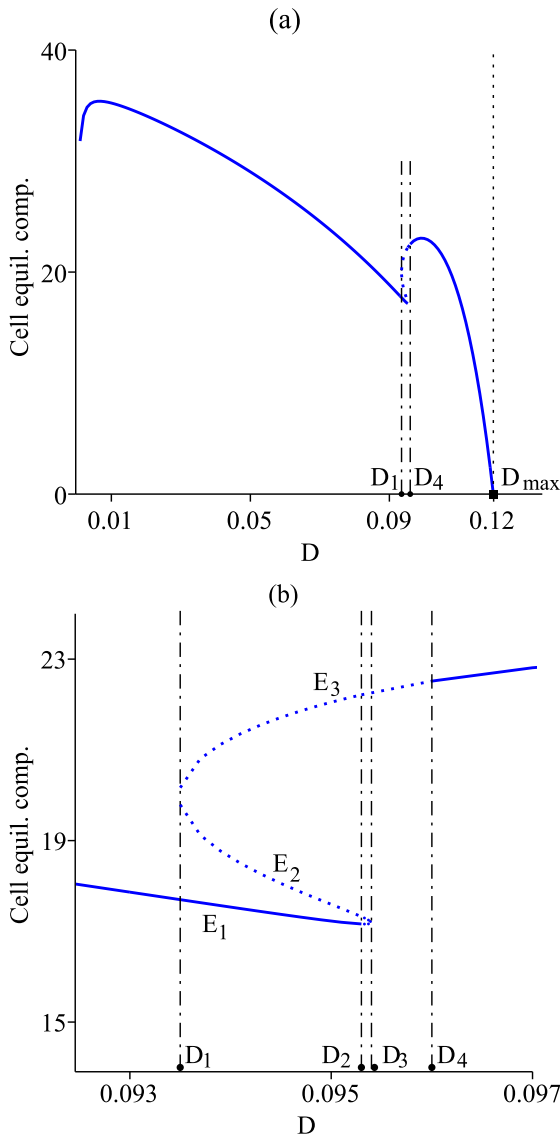
D_2. According to item (S2) there are three equilibrium points

$$E_1 = (46.67302939, 1.27619548, 17.17288338),$$
stable focus,
$$E_2 = (46.74561931, 1.36605468, 17.21665458),$$
saddle,
$$E_3 = (49.47866269, 4.66718279, 22.25755272),$$
saddle-focus,

with eigenvalues to

$$E_1 : -0.12075918, \ -0.003430554 \pm 0.02042685i,$$
$$E_2 : -0.11893152, \ -0.013142216, \ 0.029675853,$$
$$E_3 : -0.13434182, \ 0.0036402605 \pm 0.0410774i.$$

Here, starting with initial data in the basin of attraction of E_1 (i. e. in a neighborhood of E_1), the solutions are attracted by this locally asymptotically stable steady state. Figure 10 illustrates damped oscillations around E_1 using the initial point $P_2(0) = (46.67, 1.27, 17.17)$.

Figure 11 shows sustainable oscillations around the three equilibrium points E_1, E_2 and E_3 when the starting point $P_3(0) = (45, 5, 16.5)$ is relatively away from the stable steady state E_1. Since the numerical components of E_1 and E_2 are very close to each other, they are difficult to be distinguished in the plots. Please note that the inequalities $E_1 < E_2 < E_3$ are satisfied componentwise, so that in each plot the horizontal lines passing through the steady states components are ordered from bottom to top respectively.

Figures 12, 13 and 14 show projections of several trajectories in different phase planes using initial data from the set $\mathcal{P}_3(0) = \{(45, 5, 16.5), (50, 1, 18), (48, 6, 23), (55, 3, 42)\}$. Since the numerical components of the equilibria E_1 and E_2 are very close to each other, it seems from the top plots in each figure that the trajectories pass though their corresponding components. For that reason, the bottom plots in each figure visualize sufficiently large fragments of the corresponding top plots to show that the trajectories do not approach E_1 and E_2.

Example 4. $D = 0.0953960741 \in (D_2, D_3) = (0.095396073, 0.09539752)$. According to item (S2), at this value of D, relatively near to (but grater than) D_2, the following three locally asymptotically unstable equilibria exist

$$E_1 = (46.69745375, 1.30036307, 17.18187872),$$
unstable focus,

$$E_2 = (46.72951125, 1.34004418, 17.20117597),$$
saddle,
$$E_3 = (49.48610141, 4.66987416, 22.26048696),$$
saddle-focus,

with eigenvalues to

$$E_1 : -0.12013495, \ 6.148532 \times 10^{-7} \pm 0.0135992i,$$
$$E_2 : -0.0091122998, \ -0.11933523, \ 0.019457666,$$
$$E_3 : -0.13434881, \ 0.0036040251 \pm 0.041098628i.$$

Figure 15 shows projections in different phase planes of a stable limit cycle around E_1 with initial point $P_4(0) = (46.7, 1.3, 17.182)$ as a result of a *supercritical Hopf bifurcation*.

Example 5. $D = 0.0953969 \in (D_2, D_3) = (0.095396073, 0.09539752)$. For this value of D, near to D_3, there exist the following three locally asymptotically unstable equilibrium points (see item (S3)):

$$E_1 = (46.70342177, 1.30692531, 17.18469175),$$
saddle-focus,
$$E_2 = (46.72467428, 1.33323162, 17.19748187),$$
saddle,
$$E_3 = (49.48711272, 4.67023984, 22.26088530),$$
saddle,

with eigenvalues to

$$E_1 : -0.11998495, \ 0.0008949218 \pm 0.01099891i,$$
$$E_2 : -0.11945544, \ -0.0073855085, \ 0.016034111,$$
$$E_3 : -0.13434976, \ 0.003599103 \pm 0.04110151i.$$

Figure 16 visualizes the solutions and the equilibrium components (horizontal lines) with starting point $P_3(0) = (45, 5, 16.5)$. Similarly to Example 3 (see Figure 11), the components of the equilibrium points E_1 and E_2 are very close to each other, so that the inequalities $E_1 < E_2 < E_3$ should be taken into account to distinguish their components order (from bottom to top) in each plot.

Example 6. $D = 0.0957 \in (D_3, D_4) = (0.09539752, 0.0960529898)$, near to D_3. According to item (S4) there is only one locally asymptotically unstable equilibrium point

$$E_3 = (49.85615931, 4.80058160, 22.39739731),$$
saddle-focus,

with eigenvalues

$$-0.13466673, \ 0.0018647634 \pm 0.042019126i.$$

Oscillating solutions around E_3 are shown in Figure 17.

Example 7. $D = 0.096052989 \in (D_3, D_4) = (0.09539752, 0.0960529898)$. There is a unique equilibrium point

$$E_3 = (50.28183762, 4.94411687, 22.53466279),$$
$$\textit{unstable focus},$$

since its eigenvalues are

$$-0.13496827, \ 4.01863506 \times 10^{-9} \pm 0.042801144i.$$

For this value of D, near to (but less than) D_4, cf. item (S4), a stable limit cycle around the unstable focus E_3 occurs as a result of a *subcritical Hopf bifurcation* at D_4, see Figure 18.

Example 8. $D = 0.098 \in (D_4, D_{\max}) = (0.0960529898, 0.11991488)$, near to D_4. In this case (see item (S5)), there is only one locally asymptotically stable equilibrium point

$$E_3 = (52.60034923, 5.63859964, 22.98228780),$$
$$\textit{stable focus},$$

which eigenvalues are

$$-0.13578529, \ -0.0084167520 \pm 0.043929975i.$$

The solutions and the corresponding equilibrium components are shown in Figure 19.

Example 9. $D = 0.11 \in (D_4, D_{\max}) = (0.0960529898, 0.11991488)$, near to $D_{\max}$. According to item (S5), there exists a unique locally asymptotically stable equilibrium

$$E_3 = (68.24992090, 9.05274083, 17.81895944),$$
$$\textit{stable node},$$

since its eigenvalues are

$$-0.019430357, \ -0.060837981, \ -0.13004378.$$

The solutions and the corresponding equilibrium components are shown in Figure 20.

Example 10. $D = 0.13 > D_{\max} = 0.11991488$. The boundary equilibrium $E_0 = (S_A^0, S_{CP}^0, 0) = (85, 12, 0)$ is the unique locally asymptotically stable equilibrium, *a stable node*, since its eigenvalues are $-0.13, -0.13, -0.010085117$, cf. item (S6). Solutions with three initial points in the set

$$\mathcal{P}_4(0) = \{(84, 11, 21), (50, 6, 15), (30, 3, 5)\}$$

and the corresponding equilibrium components are shown in Figure 21.
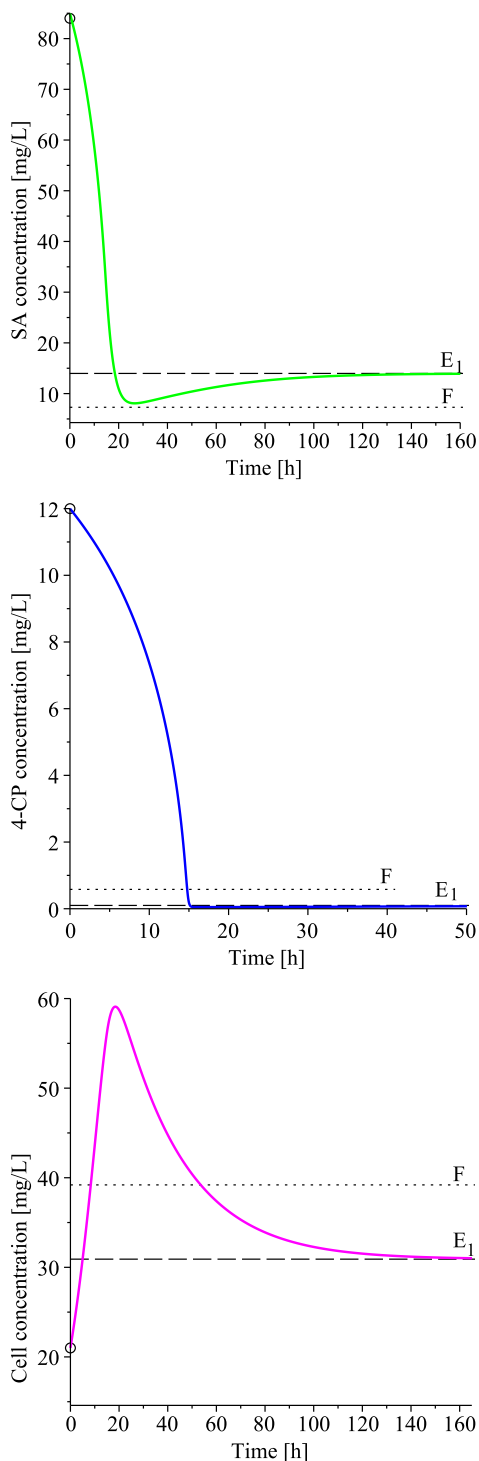
Fig. 5: Example 1: $D = 0.04 \in (0, D_1)$. Starting with the initial point $P_1(0) = (85, 12, 21)$, the solutions $S_A(t)$ (top), $S_{CP}(t)$ (middle) and $X(t)$ (bottom) tend to the equilibrium E_1 as $t \to \infty$. Initial conditions are denoted by circles on the vertical axis.
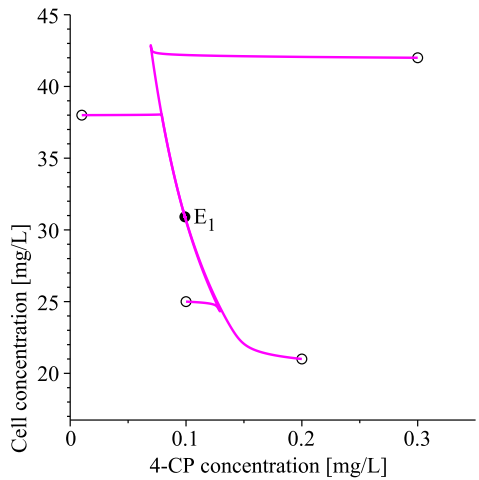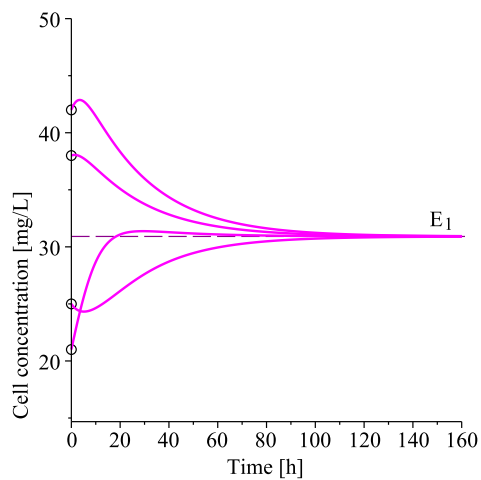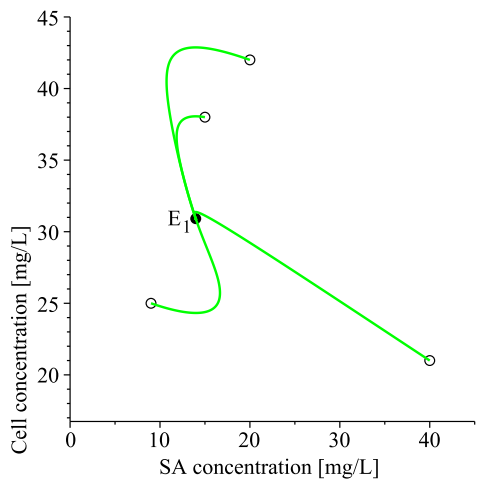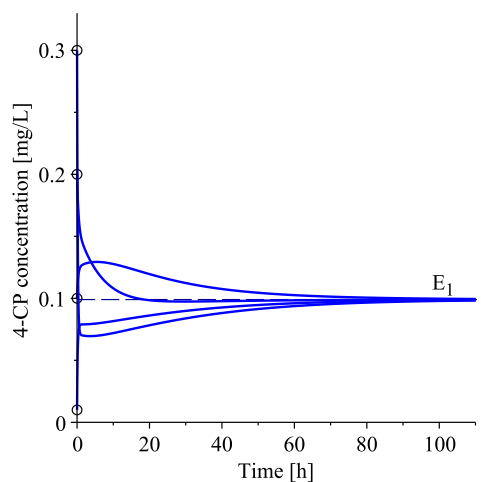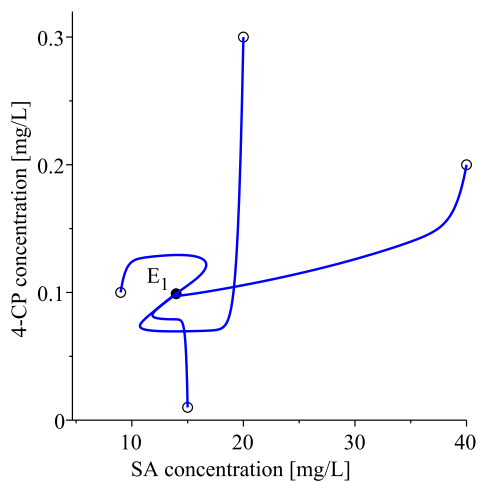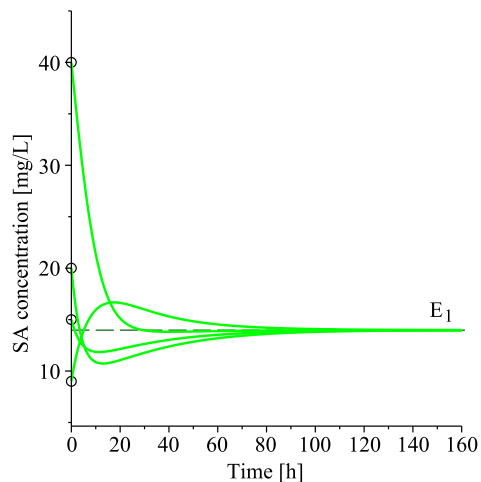
Fig. 6: Example 1: $D = 0.04 \in (0, D_1)$. Time evolution of S_A (top), S_{CP} (middle) and X (bottom) with initial conditions in the set $\mathcal{P}_1(0)$, denoted by circles.

Fig. 7: Example 1: $D = 0.04 \in (0, D_1)$. Projections of the trajectories in different phase planes with initial conditions in the set $\mathcal{P}_1(0)$, denoted by circles.
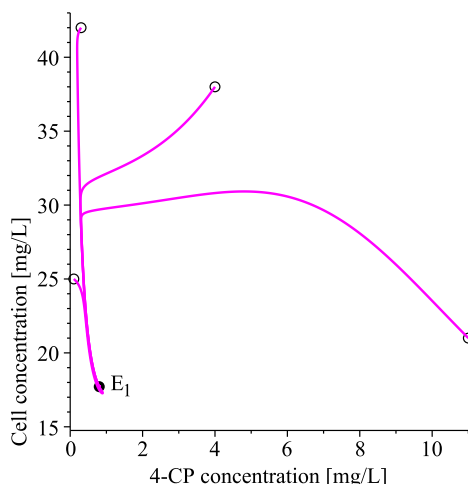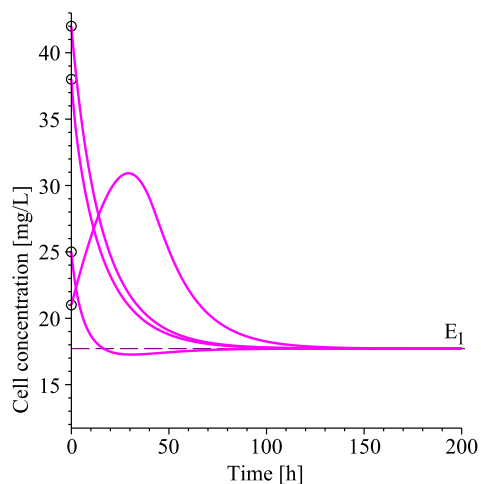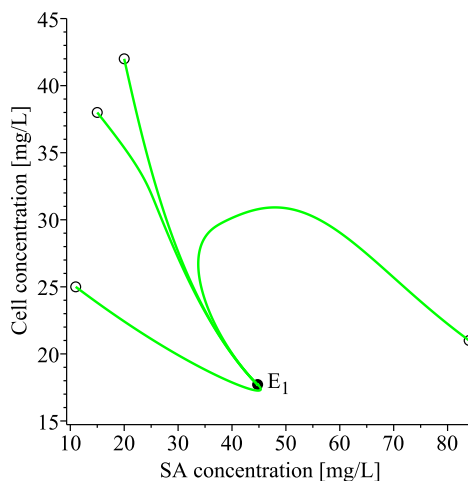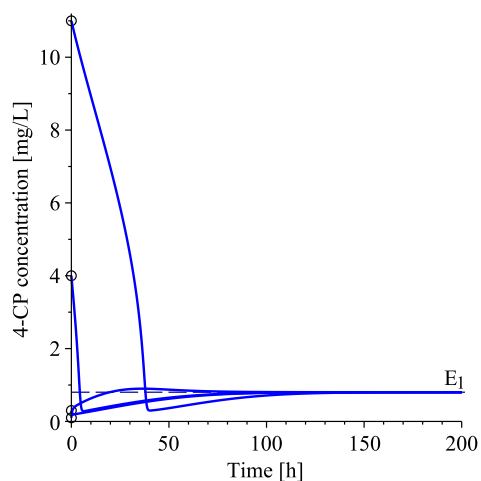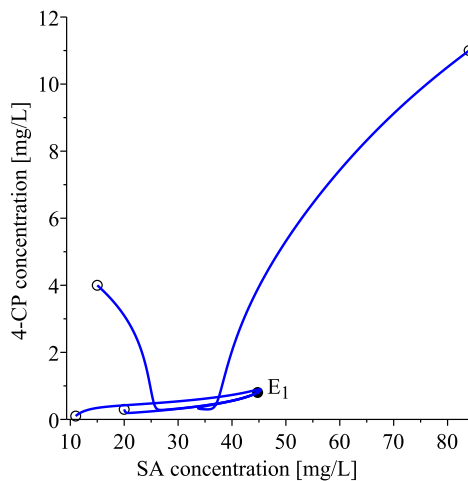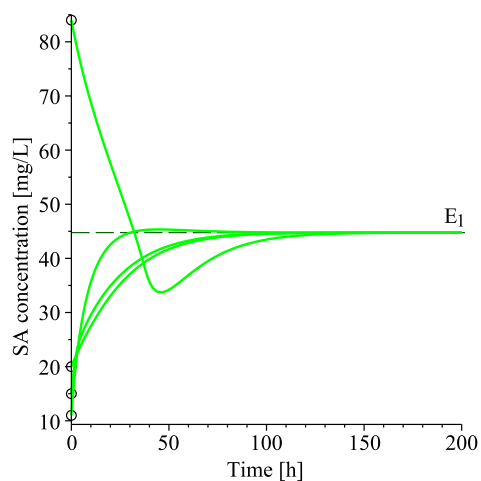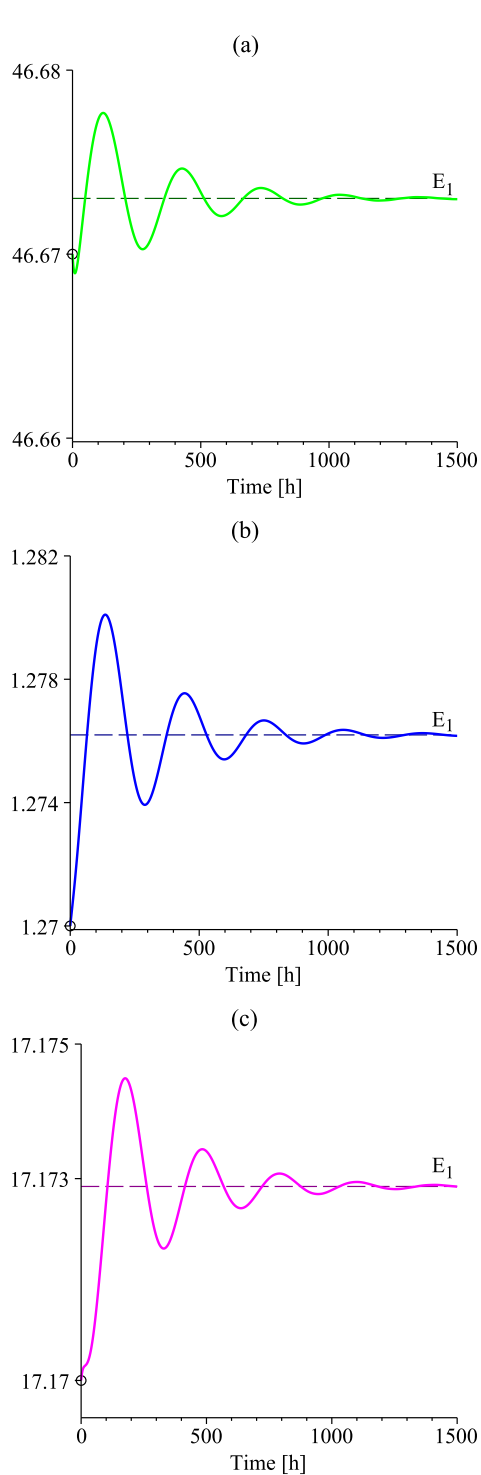
Fig. 8: Example 2: $D = 0.09345 \in (0, D_1)$. Solutions $S_A(t)$, $S_{CP}(t)$, $X(t)$ with initial conditions in the set $\mathcal{P}_2(0)$, denoted by circles.

Fig. 9: Example 2: $D = 0.09345 \in (0, D_1)$. Projections of the trajectories in different phase planes with initial conditions in the set $\mathcal{P}_2(0)$, denoted by circles.

Fig. 10: Example 3: $D = 0.09539 \in (D_1, D_2)$. Solutions: (a) $S_A(t)$, (b) $S_{CP}(t)$, and (c) $X(t)$ with initial point $P_2(0) = (46.67, 1.27, 17.17)$. The dash lines pass trough the corresponding components of the equilibrium point E_1.
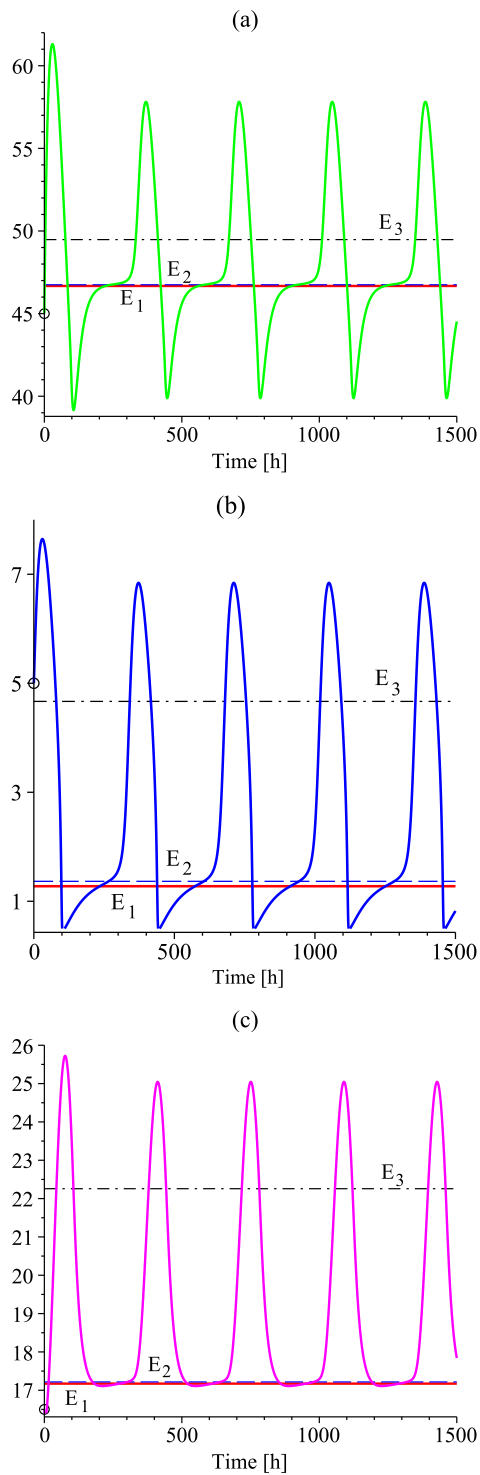
Fig. 11: Example 3: $D = 0.09539 \in (D_1, D_2)$. Solutions: (a) $S_A(t)$, (b) $S_{CP}(t)$, and (c) $X(t)$ with initial point $P_3(0) = (45, 5, 16.5)$. The horizontal lines correspond to the components of E_1 (solid red line), E_2 (dash line), E_3 (dash-dot line).
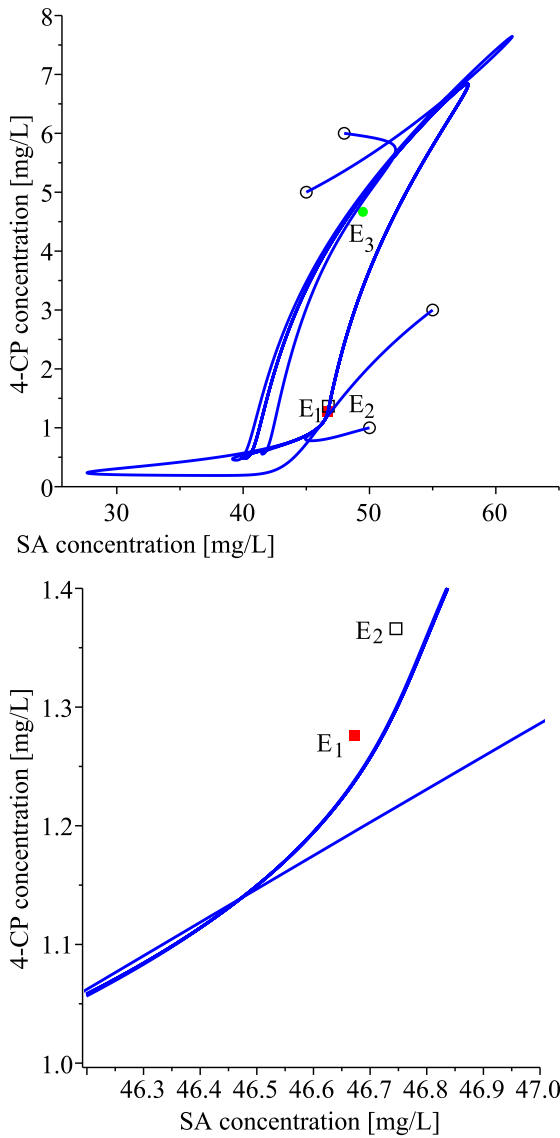
Fig. 12: Example 3: $D = 0.09539 \in (D_1, D_2)$. Projections of trajectories in the phase plane (S_A, S_{CP}) using initial data in $\mathcal{P}_3(0)$. The bottom plot presents enlarge fragment of the top plot. E_1 is marked by the red solid box, E_2—by the black box, and E_3—by the green solid circle.
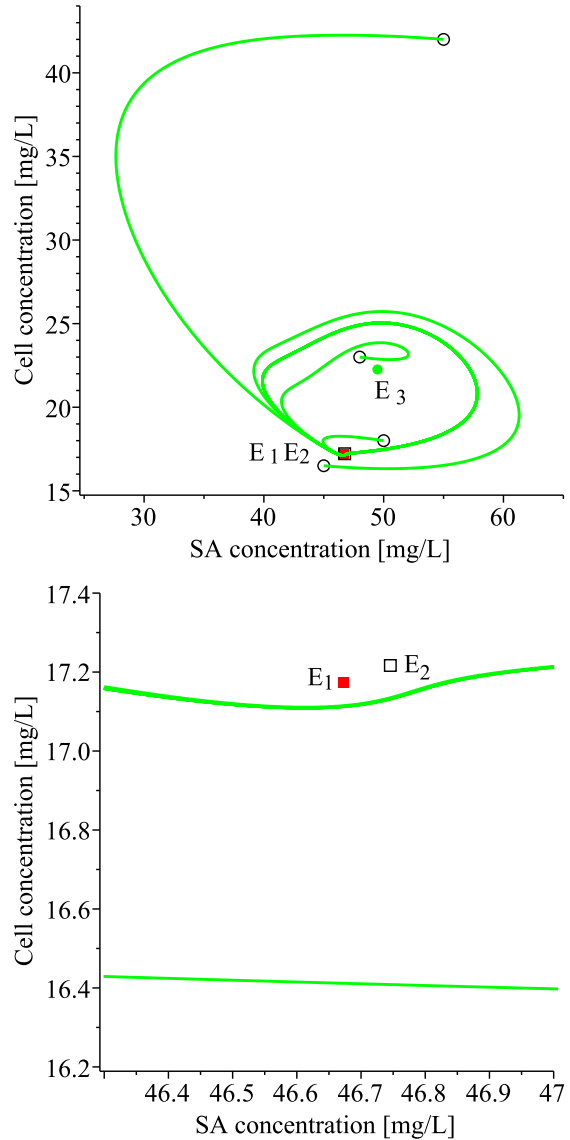
Fig. 13: Example 3: $D = 0.09539 \in (D_1, D_2)$. Projections of trajectories in the phase plane (S_A, X) using initial data in $\mathcal{P}_3(0)$. The plot below presents enlarge fragment of the top plot. E_1 is marked by the red solid box, E_2—by the black box, and E_3—by the green solid circle.
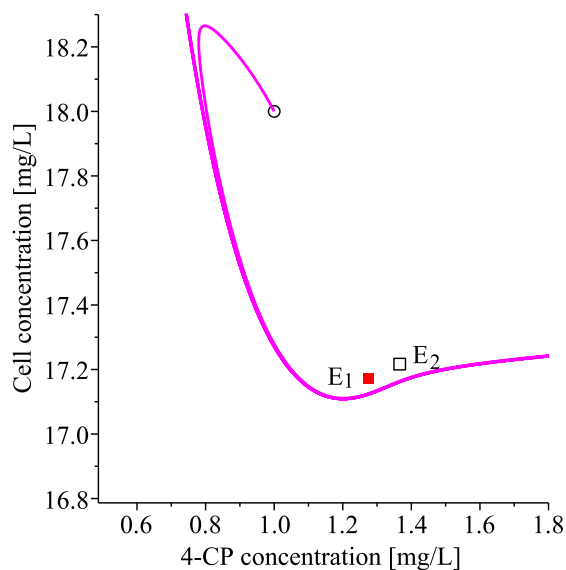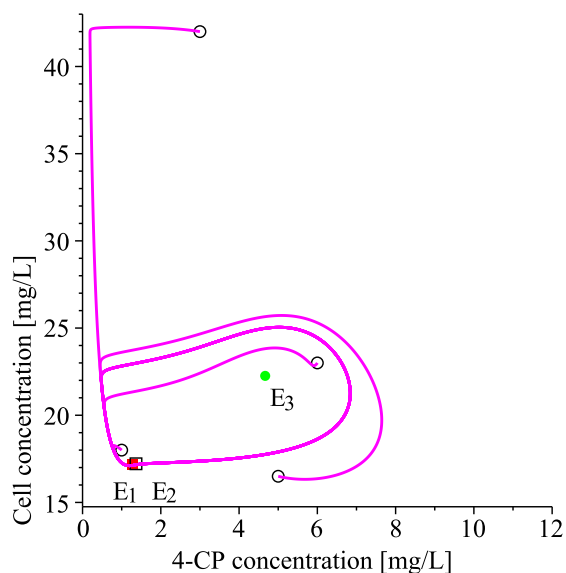
Fig. 14: Example 3: $D = 0.09539 \in (D_1, D_2)$. Projections of trajectories in the phase plane (S_{CP}, X) using initial data in $\mathcal{P}_3(0)$. The plot below presents enlarge fragment of the top plot. E_1 is marked by the red solid box, E_2—by the black box, and E_3—by the green solid circle.
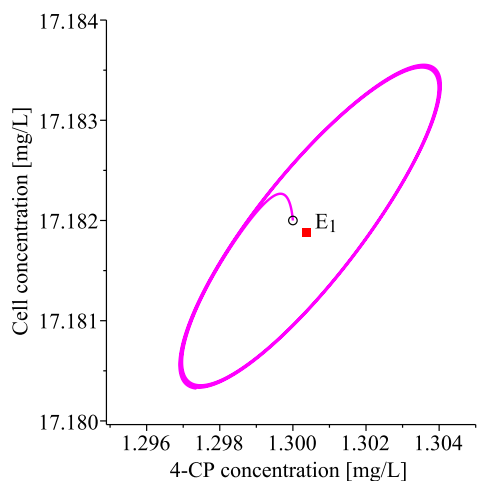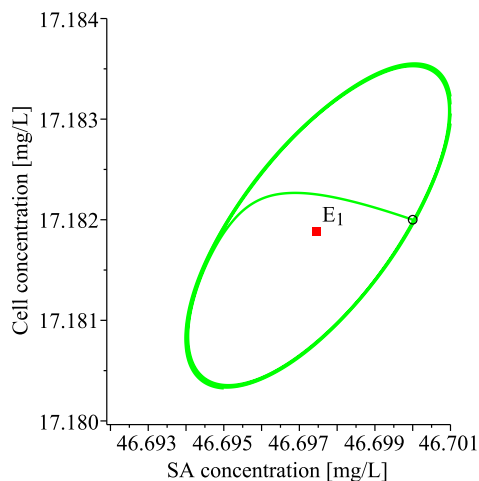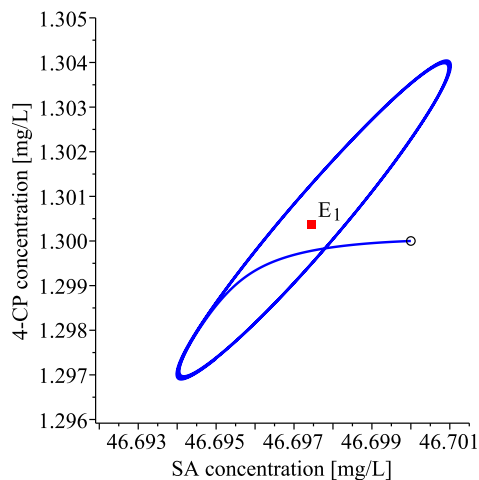
Fig. 15: Example 4: $D = 0.0953960741 \in (D_2, D_3)$. Projections of the stable limit cycle around E_1 as a result of supercritical Hopf bifurcation in different phase planes with initial point $P_4(0) = (46.7, 1.3, 17.182)$. The circles denote projections of the initial point $P_4(0)$.
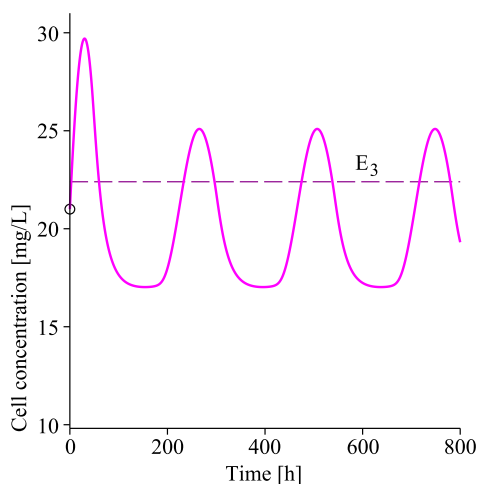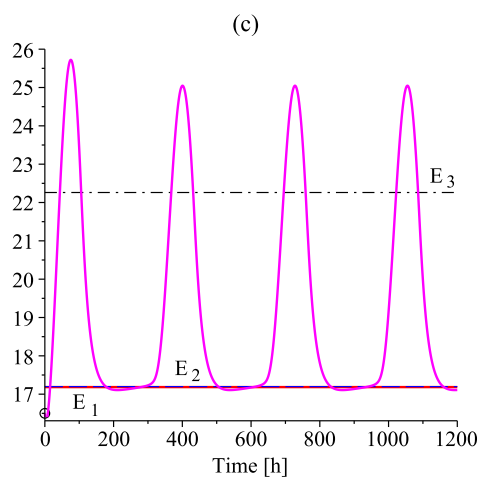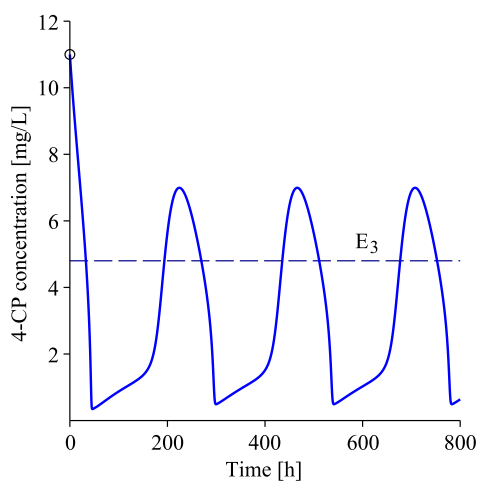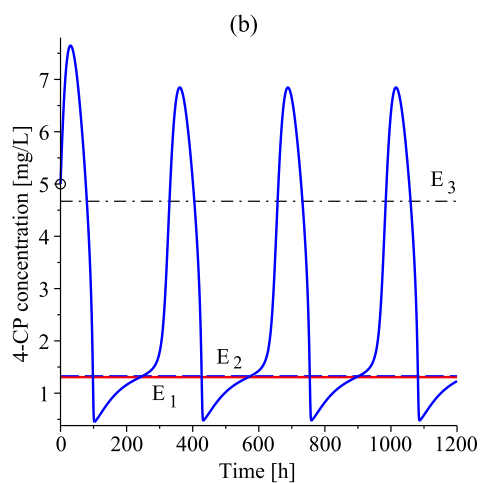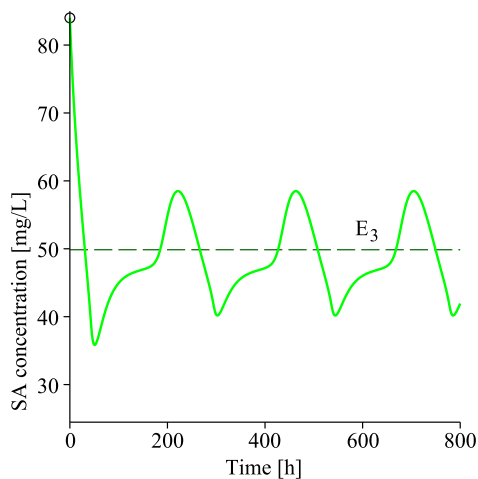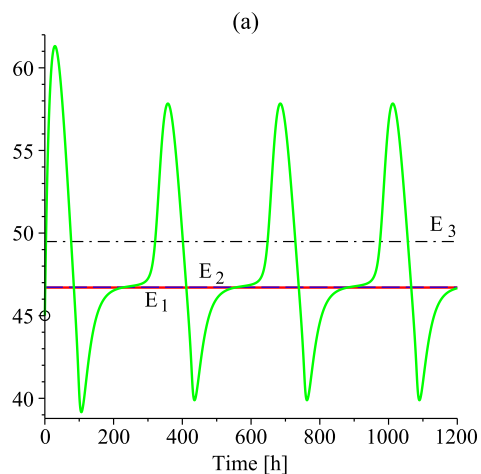
Fig. 16: Example 5: $D = 0.0953969 \in (D_2, D_3)$. Solutions (a) $S_A(t)$, (b) $S_{CP}(t)$, and (c) $X(t)$ with initial point $P_3(0) = (45, 5, 16.5)$. The horizontal lines pass through the components of the equilibrium points: E_1—solid red line, E_2—dash line, E_3—dash-dot line.

Fig. 17: Example 6: $D = 0.0957 \in (D_3, D_4)$. Solutions with initial point $P_5(0) = (84, 11, 21)$. The dash lines pass through the corresponding components of E_3.
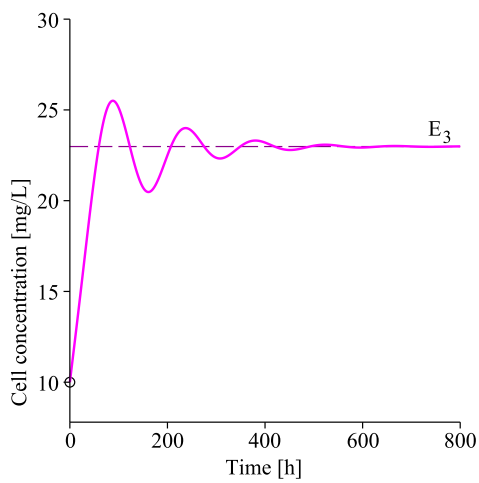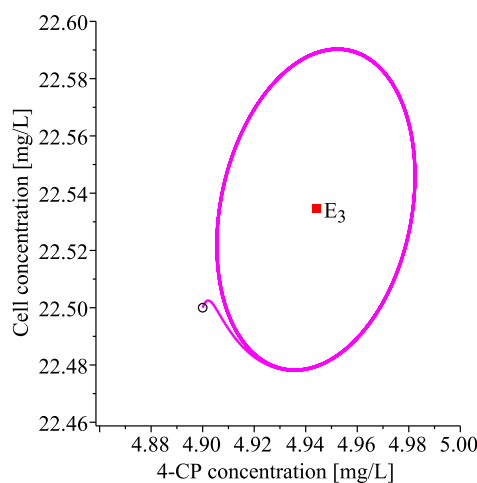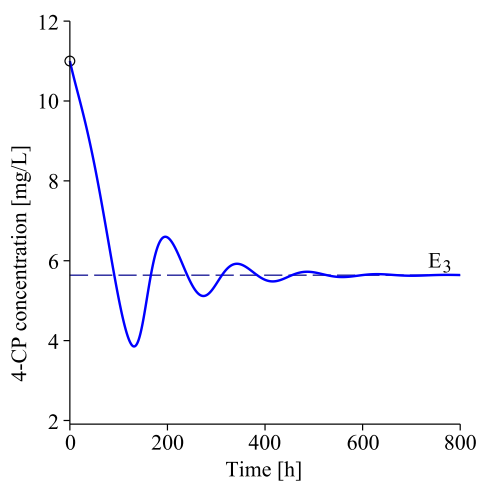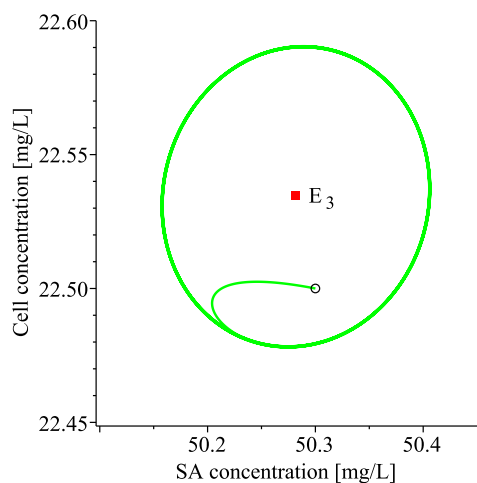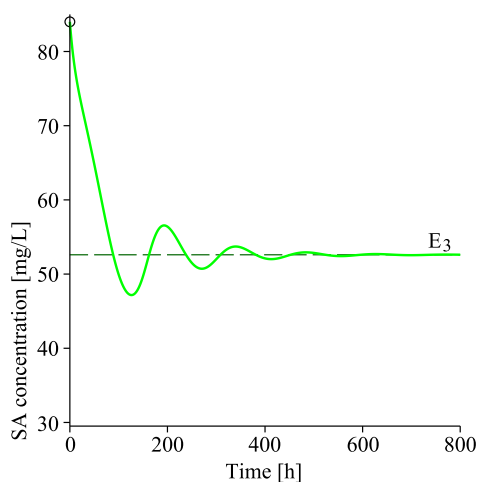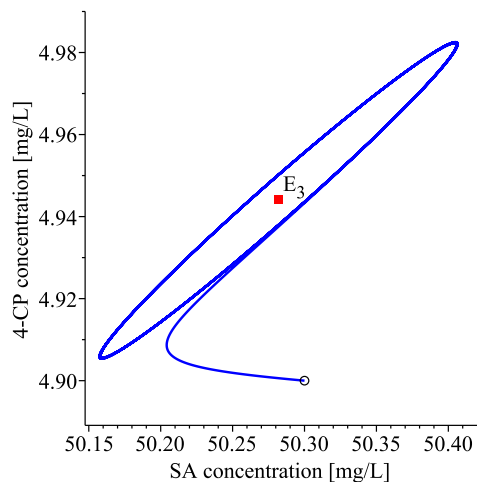
Fig. 18: Example 7: $D = 0.096052989 \in (D_3, D_4)$. Projections of the stable limit cycle around E_3 as a result of a subcritical Hopf bifurcation in different phase planes with initial point $P_6(0) = (50.3, 4.9, 22.5)$. The circles in the plots denote projections of the initial point.

Fig. 19: Example 8: $D = 0.098 \in (D_4, D_{\max})$. Initial point $P_7(0) = (84, 11, 10)$. Damped oscillations around the stable focus E_3. The dash-lines pass through the corresponding components of E_3. The circles mark the components of $P_7(0)$.
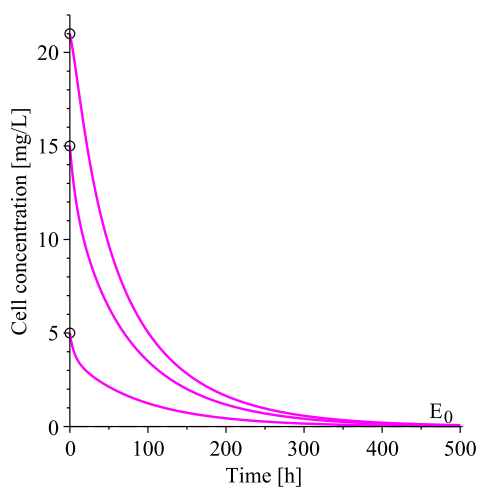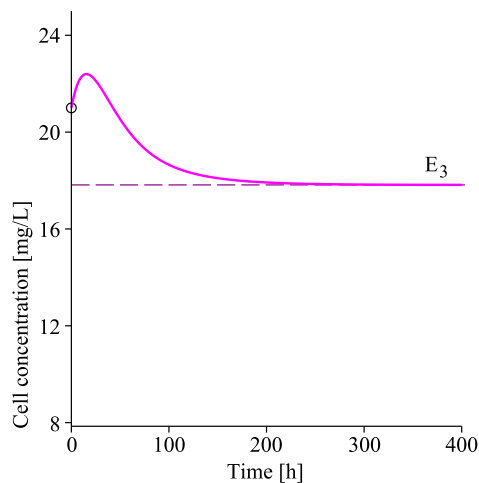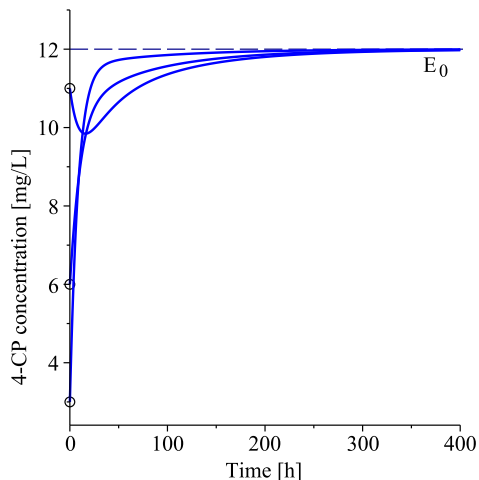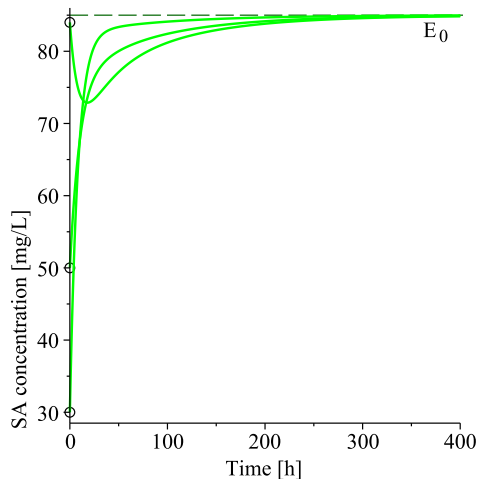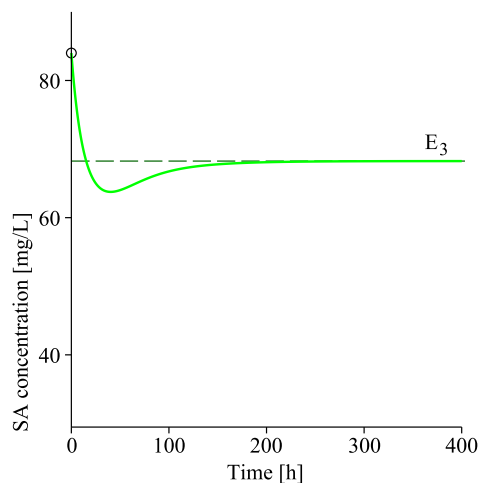
Fig. 20: Example 9: $D = 0.11 \in (D_4, D_{\max})$, initial point $P_5(0) = (84, 11, 21)$. The dash-lines pass through the corresponding components of E_3. The circles denote the components of $P_5(0)$.
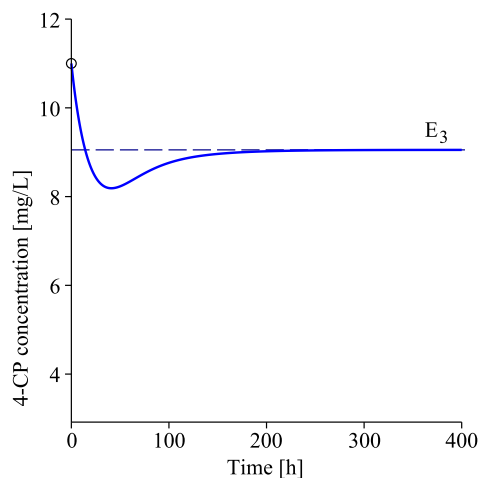
Fig. 21: Example 10: $D = 0.13 > D_{\max}$. Solutions with three different initial points in the set $\mathcal{P}_4(0)$. The dash-lines pass through the corresponding components of E_0. The circles denote the components of the initial points.

VI. DISCUSSION AND CONCLUSION

Biotechnological processes are highly complex processes, involving living microorganisms which dynamics is often unstable and not well known. Most of the controlling and monitoring techniques available in the literature are model-based and are successfully used in recent decades to predict the behavior of the systems.

This paper provides an analysis of the continuous-time model for biodegradation of 4-chlorophenol (4-CP) and sodium salicylate (SA) mixture in a chemostat by *Pseudomonas putida* cells, proposed for the first time and experimentally validated in [10]. The model is presented by a system of three nonlinear ordinary differential equations involving different and nonstandard types of kinetic models $\mu_{SA}(S_A, S_{CP})$, $\mu_{CP}(S_{CP})$ for degradation of SA and 4-CP by microorganisms as well as for the specific growth rate $\mu_X(S_A, S_{CP})$ of the cells. Some important properties of the model solutions—positivity, uniqueness and uniform boundedness—are established theoretically in Section III, Theorems 1 and 2. By numerical computations, performed in the computer algebra system *Maple*, critical values $0 < D_1 < D_2 < D_3 < D_4 < D_{\max}$ of the key model parameter D, the dilution rate, are found, so that in the intervals $(0, D_1)$, (D_1, D_2), (D_2, D_3), (D_3, D_4), $(D_4, D_{\max})$ there exist one or three interior (with positive components) admissible equilibrium points. Local stability analysis of all equilibria is provided when D belongs to each one of the above mentioned intervals. It is shown numerically that the interior steady states possess different types of local stability/instability. Two types of Hopf bifurcations—supercritical and subcritical—of the interior equilibria are also established for particular values of D. A boundary (washout with respect to biomass) equilibrium E_0 exists for all values of $D > 0$. It is shown that the latter is locally asymptotically unstable if $D < D_{\max}$ and stable for $D > D_{\max}$. Moreover, at $D = D_{\max}$ a transcritical bifurcation occurs and leads to stability exchange between an interior and the boundary steady states. These results are summarized in Table II. The dynamic behavior of the model solutions is illustrated by several numerical examples for different values of D in the environment of the software system *Maple*.

According to item (S1), for $D \in (0, D_1) = (0, 0.09348963)$ there is a unique locally asymptotically stable equilibrium point E_1, but with different stability properties. It can be shown numerically, that if $D \leq 0.0746$, then E_1 is a stable node, but for $0.0746 < D < D_1$, E_1 becomes a stable focus. In practical applications it is recommended to use values of $D \leq 0.0746$, since then the model solutions stabilize to the corresponding equilibrium in reasonable time, cf. Examples 1 and 2, otherwise some oscillations of the model solutions are possible, which may cause unpredictable behavior of the process.

At $D = 0.10845$, the unique equilibrium is $E_3 = (66.00867405, 8.62409201, 19.28481020)$. If $0.10845 \leq D < D_{\max}$ then E_3 is a stable node, whereas if $D_4 < 0.10845 < D_{\max}$ then E_3 is a stable focus (see item (S5)). In the first case of a stable node the model solutions will stabilize to E_3 in relatively small time without any oscillations (like in Figure 20). However, for these values of D, the SA and 4-CP concentrations in the chemostat remain rather high (and become higher with increasing D) and may not fall into the prescribed ecological bounds, which is not desirable in practical applications. That is why smaller values of $D < 0.0746$ are recommended to control a real-life chemostat (bioreactor) system.

REFERENCES

[1] V. Arutchelvan, R. C. Atun, Degradation of phenol, an innovative biological approach, *Advances in Biotechnology and Microbiology*, 12:555835, 2019.

[2] Y. Zhou, M. Nemati, Co-biodegradation of phenol, o-cresol, and p-cresol in binary and ternary mixtures: Evaluation of bioreactor performance and toxicity of treated effluents, *Water, Air, and Soil Pollution*, 233:133, 2022.

[3] N. Aarab, A. Essekri, H. Chafai, H. Kabli, H. Eljazouli, M. E. R. Lakhmiri, A. Albourine, Removal of sodium salicylate from aqueous solution using spruce wood sawdust as an eco-friendly adsorbent, *Mediterrian Journal of Chemistry*, 10(4):335–345, 2020.

[4] K. F. Reardon, D. C. Mosteller, J. D. B. Rogers, Biodegradation kinetics of benzene, toluene, and phenol as single and mixed substrates for *Pseudomonas putida* F1, *Biotechnology and Bioengineering*, 69(4):385–400, 2000.

[5] R. S. Juang, S. Y. Tsai, Growth kinetics of *Pseudomonas putida* in the biodegradation of single and mixed phenol and sodium salicilate, *Biochemical Engineering Journal*, 31(2):133–140, 2006.

[6] S.-Y. Tsai, R.-S. Juang, Biodegradation of phenol and sodium salicylate mixtures by suspended *Pseudomonas putida* CCRC 14365, *Journal of Hazardous Materials*, 138(1):125–132, 2006.

[7] S. Kumar, D. Arya, A. Malhotra, S. Kumar, B. Kumar, Biodegradation of dual phenolic substrates in simulated wastewater by *Gliomastics indicus* MTCC 3869, *Journal of Environmental Chemical Engineering*, 1(4):865–874, 2013.

[8] L. Zhao, Q. Wu, A. Ma, Biodegradation of phenolic contaminants: Current status and perspectives, *IOP Conference Series Earth and Environmental Science*, 111:012024, 2018.

[9] Y. Wen, C. Li, X. Song, Y. Yang, Biodegradation of phenol by *Rhodococcus* sp. strain SKC: Characterization and kinetics study, *Molecules*, 25:3665, 2020.

[10] Y.-H. Lin, B.-H. Ho, Biodegradation kinetics of phenol and 4-chlorophenol in the presence of sodium salicylate in batch and chemostat systems, *Processes*, 10:694, 2022.

[11] H. L. Smith, P. Waltman, *The Theory of the Chemostat: Dynamics of Microbial Competition*, Cambridge University Press, Cambridge, 1995.

[12] J. Harmand, C. Lobry, A. Rapaport, T. Sari, *The Chemostat: Mathematical Theory of Microorganism Cultures*, Chemical Engineering Series Volume 1, John Wiley and Sons, 2017.

[13] M. Borisov, N. Dimitrova, P. Zlateva, Time-delayed bioreactor model of phenol and cresol mixture degradation with interaction kinetics, *Water*, 13:3266, 2021.

[14] N. Dimitrova, P. Zlateva, Global stability analysis of a bioreactor model for phenol and cresol mixture degradation, *Processes*, 9:124, 2021.

[15] M. Borisov, N. Dimitrova, P. Zlateva, Stability analysis of a chemostat model for phenol and sodium salicylate mixture biodegradation, *Processes*, 10:2571, 2022.

[16] K. C. Loh, Y. G. Yu, Kinetics of carbazole degradation by *Pseudomonas putida* in presence of sodium salicylate, *Water Research*, 34(17):4131–4138, 2000.

[17] S. J. Wang, K. C. Loh, S. S. Chua, Prediction of critical cell growth behavior of *Pseudomonas putida* to maximize the cometabolism of 4-chlorophenol with phenol and sodium glutamate as carbon sources, *Enzyme and Microbial Technology*, 32:422–430, 2003.

[18] Q. Wang, Y. Li, J. Li, Y. Wang, C. Wang, P. Wang, Experimental and kinetic study on the cometabolic biodegradation of phenol and 4-chlorophenol by psychrotrophic *Pseudomonas putida* LY1, *Environmental Science and Pollution Research*, 22:565–573, 2015.

[19] J. Wang, Z. Sun, Exploring the effects of carbon source level on the degradation of 2,4,6-trichlorophenol in the co-metabolism process, *Journal of Hazardous Materials*, 392:122293, 2020.

[20] J. K. Hale, *Ordinary Differential Equations*, Krieger Publishing Company, 1980.

[21] S. Wiggins, *Introduction to Applied Nonlinear Dynamical Systems and Chaos*, Second Edition, Texts in Applied Mathematics Volume 2, Springer, New York, 1990.